Axion physics in condensed-matter systems

Dennis M. Nenno[1,2]✉, *Christina A. C. Garcia*[2], *Johannes Gooth*[1,3], *Claudia Felser*[1,2] *and Prineha Narang*[2]✉

Abstract | Axions are hypothetical particles that were proposed to solve the strong charge–parity problem in high-energy physics. Although they have long been known in quantum field theory, axions have so far not been observed as elementary particles in nature. Yet, in condensed-matter systems, axions can also emerge as quasiparticles in certain materials such as strong topological insulators. The corresponding axion field is expected to lead to exciting physical phenomena in condensed-matter systems, such as a fractional quantum anomalous Hall effect, the chiral anomaly, exotic Casimir–Lifshitz repulsion and a linear magnetoelectric response quantized in units of the fine-structure constant. First signatures of electronic states that permit axion dynamics have been reported in condensed-matter systems. In this Review, we explore the concepts that introduce axion fields in condensed-matter systems and present experimental findings. We discuss predicted and realized material systems, the prospects of using axion electrodynamics for next-generation devices and the search for axions as a possible constituent of dark matter.

$\mathbb{Z}_2$ invariant
Group of integers 0, 1 first introduced in 2D time-reversal-invariant systems to distinguish topological from trivial phases.

The concepts of the axion field and its fundamental excitation — the axion particle — were first introduced more than 40 years ago to explain the absence of charge–parity violation in the strong interaction between quarks[1,2]. Since then, it has been adopted in string theory and cosmology, and the axion particle has become a current candidate for dark matter[3], although no traces of the elementary axion particle have yet been observed. Axions are introduced by an additional term in the laws of electrodynamics, which rotates the electric and magnetic fields into each other. In 1987, Frank Wilczek proposed that similar laws of electrodynamics could potentially be observed in condensed-matter systems[4]. Twenty years later, it was discovered that a term analogous to the one that would be added to Maxwell's equations to account for elementary axions does indeed appear in the description of certain topological materials[5–8], giving rise to an effective axion description of the electrodynamics in these systems.

The study of topological materials is one of the most active fields of research in modern condensed-matter science[9,10], and it is believed that at least a quarter of all known materials have topological properties[11]. The field started with the prediction and realization of topological insulators (TIs), materials that are insulating in the bulk but show quantized, dissipationless metallic states on their surfaces[12–15]. At a fundamental level, TIs are characterized by quantized responses that are stable with respect to perturbations or continuous transformations. Topological field theories can predict the responses of these materials irrespective of microscopic details, making assumptions only about the symmetries of the system. Among them, time-reversal-invariant insulators in 3D form a class that can be divided into 'strong' and 'weak' TIs, as well as 'trivial' insulators, by an integer value derived from their band structure, the '$\mathbb{Z}_2$ invariant'[16]. This classification was extended to systems that break time-reversal symmetry, such as antiferromagnetic TIs[17]. The electromagnetic coupling governed by the axion field in these structures provides one method of calculating the $\mathbb{Z}_2$ invariant, with a direct physical interpretation[5,17].

In a strong TI, the effective axion term derived from its electronic states can lead to unique responses under certain conditions. Among them, the topological magnetoelectric effect results in a linear coupling between electric and magnetic fields[5,6,18]. This effect leads to an induced electric polarization when applying a magnetic field and a magnetization when applying an electric field. The fact that this linear coupling is present even in centrosymmetric or time-reversal-invariant materials is a striking physical consequence, as there exist only a few well-studied materials that exhibit such a coupling[5,19]. In addition, the quantum anomalous Hall effect that naturally arises in magnetic TIs can be readily explained by the surface current response obtained from axion

[1]*Max Planck Institute for Chemical Physics of Solids, Dresden, Germany.*
[2]*John A. Paulson School of Engineering and Applied Sciences, Harvard University, Cambridge, MA, USA.*
[3]*Institut für Festkörper- und Materialphysik, Technische Universität Dresden, Dresden, Germany.*
✉*e-mail:* *nenno@seas.harvard.edu*; *prineha@seas.harvard.edu*

https://doi.org/10.1038/s42254-020-0240-2

Key points

- 3D insulators can be topologically characterized by the value of their bulk axion field.
- Axion fields introduce additional terms in Maxwell's equations for condensed-matter systems.
- The microscopic expression for the axion field in a crystal is given by the non-Abelian Chern–Simons integral, which depends on the Berry connection matrix of the band structure.
- In strong 3D topological insulators, a half-quantized surface Hall effect appears when the surface states are gapped, together with linear magnetoelectric coupling in their bulk.
- The axion insulator state can be realized in antiferromagnetic insulators without external fields.
- Materials with a non-trivial axion field can be used in dark-matter detectors and non-reciprocal thermal emitters.

electrodynamics[5]. The microscopic expression that determines the axion field takes quantized values of 0 or π in time-reversal-invariant insulators, providing a topological classification equivalent to the $\mathbb{Z}_2$ invariant in three dimensions. Furthermore, in structures that lack time-reversal symmetry, spatial or composite symmetries can also quantize the axion field[5,6,17,20]. Axion domain walls appear at interfaces and surfaces of these materials and eventually lead to half-quantized Hall responses[5,21]. Compared with its elementary version in high-energy physics, the condensed-matter realizations of the axion have the advantage of being directly accessible in magnetoelectric experiments.

It was only a few years after the discovery of 3D TIs that axion electrodynamics was proposed to govern the electromagnetic response in Weyl semimetals as well[7,8]. The chiral anomaly related to this response had already been predicted to arise in the early 1980s (REF.[22]). The realization of Weyl semimetals, as well as their response, has been the subject of several excellent reviews[23–26], so we centre our discussion around insulating materials.

The electronic states in materials that contribute to the axion field have not only been studied in the originally proposed bismuth-based alloys[5,27] but have now also been observed in, among others, charge-density-wave Weyl semimetals[28], antiferromagnetic insulators[17,29,30] and topological heterostructures[31–33]. In these materials, experiments have been able to probe signatures of the peculiar electrodynamics that lead to a quantized topological response[34–37]. However, even though the basis in terms of suitable materials and structures is established, a direct observation of the topological magnetoelectric effect is still missing. Its quantization of the interaction in units of the fine-structure constant makes a direct measurement a desirable goal for experimentalists.

Our Review provides an introduction to the topic of axion electrodynamics in condensed-matter systems. In particular, we focus on the resulting phenomena in TIs, comment briefly on the chiral anomaly as manifestation of axion electrodynamics in Weyl semimetals and discuss potential material systems for the realization of the resulting physics. We highlight recent experiments in candidate axion insulator systems and close the Review with a discussion of applications of axion insulator materials for dark-matter detection, non-reciprocal emission and their connection to other topological devices.

Chern number
Berry flux on a closed manifold, which becomes quantized in time-reversal-breaking topological insulators.

Berry connection
Gauge-dependent vector potential connected to the Berry phase.

Topological field theory

Particle physics formulates its governing laws in terms of quantum field theories, in which particles are described as quantized excitations of the field. The standard model of particle physics can be stated in terms of its Lagrangian, which controls the dynamics and interaction of elementary particles. As mentioned in the introduction, the term accounting for the axion is added to the Lagrangian of the standard model to solve the strong charge–parity problem[2,38]. We now discuss how this additional term arises naturally in strong TIs in three dimensions, how it leads to a topological classification in materials that break time-reversal symmetry and how it is connected to the formal polarization. The physical effects of the coupling can manifest themselves in half-quantized surface states and the topological magnetoelectric effect. In Weyl semimetals, an axion term arises from the separation of the chiral band crossings in momentum space and energy[7,8,22]. Furthermore, the condensed-matter realization of axion electrodynamics is a fascinating example in which the low-energy contribution to the field (the 'axion angle') can be determined by the microscopic theory.

With the discovery of the quantum Hall effect — the quantized version of the Hall effect arising in a 2D electron gas subject to a strong magnetic field — the concept of topology was introduced in the description of electronic states in condensed-matter systems[39,40]. David Thouless, Mahito Kohmoto, Marcel den Nijs and Peter Nightingale (TKNN) realized that individual Bloch bands u_j yield quantized contributions to the Hall conductivity,

$$n_j = \frac{i}{2\pi}\int_{\mathrm{BZ}} \mathrm{d}^2k \left(\left\langle \partial_{k_y} u_j \middle| \partial_{k_x} u_j \right\rangle - \left\langle \partial_{k_x} u_j \middle| \partial_{k_y} u_j \right\rangle \right), \quad (1)$$

where the integral runs over the Brillioun zone (BZ) of the crystal, with the quasi-momentum axis k. The contributions from occupied bands can be added together to obtain the total Hall conductivity,

$$\sigma_{xy} = \frac{e^2}{h} \sum_{j\in \mathrm{occ}} n_j = \frac{e^2}{h} C_1. \quad (2)$$

The sum of all n_j is called the TKNN invariant or first Chern number (C_1) and provides an integer classification of the system which is observable in experiment. This result can be obtained from standard perturbation theory for Bloch states $u_{m,n}$ and written in terms of the Berry connection,

$$a_\mu^{mn}(\mathbf{k}) = -i \left\langle u_m(\mathbf{k}) \middle| \frac{\partial}{\partial k_\mu} \middle| u_n(\mathbf{k}) \right\rangle, \quad (3)$$

as $C_1 = 1/(2\pi)\int \mathrm{d}^2k(\partial_{k_x} a_y - \partial_{k_y} a_x)$. The quantum Hall state resides in a topologically non-trivial Hilbert space, and its Chern number C_1 provides an invariant

that specifies the system. Its electromagnetic action is described by a Chern–Simons term[5]

$$S_{\text{eff}}^{\text{2D}} = \frac{C_1}{4\pi}\int \mathrm{d}^2x \int \mathrm{d}t\ \varepsilon^{\mu\nu\tau}A_\mu\partial_\nu A_\tau. \tag{4}$$

Here, ε denotes the Levi–Civita symbol, and we sum over spatiotemporal indices in (2 + 1) dimensions ($\mu,\nu,\tau = t,x,y$). The external vector field is denoted by A, and ∂_ν takes its spatial derivative along ν. The coupling constant C_1 to the field theory provided by Eq. (4) is exactly the first Chern number, which again is identified by the microscopic details of the system, encoded in the Bloch bands and the Berry connection, Eq. (3). From the action, one can recover the response of the current to an external potential A (REF.[5]),

$$j^\mu = \frac{C_1}{2\pi}\varepsilon^{\mu\nu\tau}\partial_\nu A_\tau, \tag{5}$$

from which the quantized Hall effect, Eq. (2), can immediately be obtained. The quantum Hall system is the first realization of a class of materials called TIs, as its bulk states are gapped in the presence of an external magnetic field, whereas its surface is characterized by chiral gapless states.

In 2005, the introduction of the quantum spin Hall effect generalized the idea of topology to the time-invariant case[16]. The quantum spin Hall insulator was proposed as a new type of band insulator with two spin channels that are coupled by the spin–orbit interaction on a graphene lattice. The presence of time-reversal symmetry in this system results in its electronic structure having topologically protected non-trivial character, making it the first predicted symmetry-protected topological phase. Such a phase was both predicted and experimentally observed in cladded HgTe structures in the following 2 years[41,42]. Time-reversal-invariant TIs in two and three dimensions can be classified by their $\mathbb{Z}_2$ invariant, an integer value that is either 0 or 1, separating trivial from topological states. A brief expression for the topological invariant ν, sometimes referred to as the Fu–Kane formula, is based on the Pfaffian of the system, Pf (REFS[43,44]),

$$(-1)^\nu = \prod_{j=1}^{4}\frac{\sqrt{\mathrm{Det}[w(\Gamma_j)]}}{\mathrm{Pf}[w(\Gamma_j)]}, \tag{6}$$

where Det is the determinant, Γ_j the four time-reversal-invariant momenta in two dimensions and w is defined by

$$w_{mn}(\mathbf{k}) = \langle u_m(\mathbf{k})|\mathcal{T}|u_n(-\mathbf{k})\rangle. \tag{7}$$

The argument of the Pfaffian, w, calculates the overlap between states in different bands under time reversal, $\mathcal{T}$, and is consequently sensitive to degeneracies. The Pfaffian exists because w in Eq. (7) is an antisymmetric matrix. The $\mathbb{Z}_2$ invariant ν can take only two values, 0 and 1, and, although it remains a bulk quantity evaluated from its Bloch bands, this bulk topological index decides the existence of non-trivial surface states. Inversion symmetry can further aid the calculation of ν, as only special points of the Brillouin zone have to be considered in this case[45]. Several excellent reviews elaborate on the derivation of schemes to calculate this invariant from the entire bulk or specific points of the band structure[9,10]. In practice, a feasible way to calculate the $\mathbb{Z}_2$ invariant is to track centres of the Wannier charge, elaborated on in REFS[46,47].

To realize a $\mathbb{Z}_2$-insulator in three dimensions, one possibility is to stack layers of quantum spin Hall insulators. The additional dimension yields three different invariants for each spatial component. This turns out to be insufficient to describe the topology of the entire system, as six individual numbers for every surface of a cube are required; however, because these surfaces are not independent, four quantities are able to fully characterize the topology of a 3D insulator, usually written as the set (ν_0; $\nu_1\nu_2\nu_3$) (REFS[14,45]). If the first index is odd, the material is a strong TI; if it is even and at least one of the latter three is odd, it is understood to be a weak TI. Weak TIs have an even number of conducting Dirac cones on the surface, whereas strong TIs show an odd number of surface cones. Both cases are topologically non-trivial states in the clean limit, that is, for systems with unperturbed bulk states, in which they show the bulk–boundary correspondence, exhibiting metallic surface states[48,49].

The first strong TI was experimentally identified by angle-resolved photoemission in $Bi_{1-x}Sb_x$ compounds, despite a relatively small bulk gap of the order of thermal excitations[50]. Using the same technique, a single Dirac cone on the surface of the otherwise insulating Bi_2Te_3 was identified, providing the first observation in the predicted family of Bi_2Te_3 and Sb_2Te_3 compounds[51]. Bi_2Te_3 is the heaviest combination in this family and establishes a bandgap of 0.3 eV, rendering it a prototype material in this field. Many more topological compounds have been identified, synthesized and measured in recent years, opening a wide field of research[9–11,52].

Axion coupling

In an effort to unify the different topological quantities in two and three dimensions, a field theory was introduced based on the nonlinear response of an imaginary (4 + 1)-dimensional TI[5]. In a spirit similar to the derivation of the first Chern number from linear perturbation theory, an expression for the second Chern number is derived, which appears as a nonlinear response coefficient. For (4 + 1) dimensions, the second Chern number, C_2, is directly analogous to the TKNN invariant in (2 + 1) dimensions in describing the response of a current to an external field. By dimensional reduction — choosing one of the four momentum directions and its coupling to the vector potential as an additional parameter — one obtains both a closed expression for the second Chern number and a pseudoscalar polarization term that couples nonlinearly to the external fields **E** and **B**. The coupling to the vector potential generating these fields, A, is given by the effective action in (3 + 1) dimensions[5].

$$S_{\text{eff}}^{\text{3D}} = \frac{1}{4\pi}\int \mathrm{d}^3x \int \mathrm{d}t\ \varepsilon^{\mu\nu\sigma\tau}\theta(\mathbf{x},t)\partial_\mu A_\nu\partial_\sigma A_\tau, \tag{8}$$

Kramers degeneracy
In time-reversal-symmetric systems, every energy state is at least two-fold degenerate.

again using ε to denote the Levi–Civita symbol. Equation (8) formally introduces the axion field θ, which is defined by a Chern–Simons form similar to that of the (2 + 1)-dimensional action in equation (4):

$$\theta = -\frac{1}{4\pi}\int_{\mathrm{BZ}} \mathrm{d}^3k\ \varepsilon^{\mu\nu\sigma}\mathrm{tr}\left[a_\mu\partial_\nu a_\sigma - \frac{2i}{3}a_\mu a_\nu a_\sigma\right]. \qquad (9)$$

The trace runs over the band index of the Berry connection, a, between occupied bands. We call θ an axion field in analogy with its interpretation as a fundamental gauge potential in high-energy physics. Its quantized excitations are consequently called axions. In the condensed-matter context, θ can also be interpreted as a contribution to the magnetoelectric polarization from extended orbitals[5,6,53]. This contribution to the polarization is derived from an integral over the Berry curvature tensor and arrives at an expression similar to equation (8)[6], and REF.[54] provides an excellent overview about the interpretation of the axion field as a constituent of the microscopic polarizability.

As θ is obtained as the result of integrating a 3D Chern–Simons term, it is only defined modulo 2π (REFS[5,6,54]). In the time-reversal-invariant insulator discussed above, θ can take only two values, 0 for trivial insulators and π for strong TIs, and it thus provides a $\mathbb{Z}_2$ classification.[5] In fact, in any pseudoscalar-symmetric crystal, a crystal in which a symmetry is present that reverses the sign of a pseudoscalar, θ can only take these two values in the bulk of the material[55]. Insulators with $\theta = \pi$ protected by such a symmetry that is not time reversal are called axion insulators. The surfaces of these materials are naturally gapped[56], and a further elaboration on the equivalence between $\mathbb{Z}_2$ and θ can be found in REF.[57]. An overview of topological classification schemes is shown in BOX 1.

Magnetic materials are not included in conventional classifications for 3D TIs, as their ground states break time-reversal symmetry, and the key to establish a $\mathbb{Z}_2$ classification is the existence of Kramers degeneracy[58]. However, whereas ferromagnetism breaks time-reversal symmetry, it can be shown that for almost all states, degeneracy is ensured in an antiferromagnet if there is an additional operation that connects lattice sites with opposite spin[58]. Topological antiferromagnets are now an active area of research[13,59]. Usually, a half-lattice translation $\tau_{1/2}$ connects the different sites that build a staggered Zeeman field and can be combined with time reversal to create an anti-unitary operator. We elaborate on this using the example of the recently proposed $MnBi_2Te_4$ structure later in the text.

Half-quantized interface conductance

From Eq. (8), a number of exciting physical phenomena follow, many of which have been proposed in REF.[5]. We now review some of the effects that arise for static axion fields, before turning to dynamical phenomena. One of the most interesting features and a direct consequence of a quantized axion field in the bulk is the occurrence of a half-quantized Hall effect on the surface of a strong TI, provided that the interface breaks time-reversal symmetry and gaps the surface states. Such an interface can be interpreted as an axionic domain wall, as it separates regions with $\theta = \pi$ and $\theta = 0 \bmod 2\pi$ (REFS[4,55]). One can show that the action, Eq. (8), yields a half-quantized surface Hall conductance, which in general is given by $(1/2 + m)e^2/h$. While the odd number of surface Dirac cones contributes a half Hall quantum, the second part stems from an arbitrary number $m \in \mathbb{Z}$ of quantum Hall effects on the surface[60]. When the surface states are gapped by a time-reversal-breaking perturbation, such as an external magnetic field or cladding with an insulating magnetic material, the surface Hall conductance becomes[5,61]

$$\sigma_{xy} = \pm\frac{e^2}{2h}, \qquad (10)$$

where the sign depends on the time-reversal-breaking field. This result can be observed in experiment as follows. Suppose the surfaces of a strong TI are sandwiched between two ferromagnetic insulators. Given that the magnetizations of the top and bottom ferromagnets are parallel, one expects to measure one quantum Hall conductance, as both surfaces contribute half a quantum. If the magnetization in one of the layers is now reversed, the currents on the side surfaces cancel, and a zero Hall plateau is obtained[5]. The two scenarios are depicted in FIG. 1a,b. In experiment, this effect can only be observed if the magnetically induced gap is larger than the thermal energy and if the chemical potentials of both the top and bottom surfaces lie within that gap. Heterostructures of

Box 1 | **Topological classification**

Materials can be classified by the topology of their quantum mechanical wavefunctions. A general classification scheme categorizes topological insulators (TIs) in the independent particle regime depending on their non-spatial, anti-unitary symmetries. Time-reversal and charge-conjugation (particle–hole) symmetry, together with their combination (chiral symmetry), yield ten different categories. These are the ten Altland–Zirnbauer symmetry classes (excerpt shown in the table), which depend on the sign of the symmetry of the Hamiltonian[160,161]. The topological classification of a system within one category is then defined by the homotopically inequivalent maps from momentum space (parametrized by **k**) to the Hamiltonian. 2D time-reversal symmetry breaking insulators are characterized by the first Chern number $C_1 \in \mathbb{Z}$ and fall into class A. 2D and 3D TIs that have time-reversal symmetry can both be characterized by a $\mathbb{Z}_2$ number and fall into class AII. The difference between these classes can be understood through the difference in the transformation of the action integral under charge conjugation and time reversal[5], and, as the action integral is exactly a Chern–Simons form, such transformations are well understood mathematically[162–164]. In general, Chern numbers are the coefficients of the Chern–Simons action integral in d dimensions, where the coefficient in the latter is the $d/2$-Chern number[5,60]. A physically intuitive picture of this topic is presented in REF.[60].

Introducing spatial symmetries into the classification scheme makes it possible to derive simplified expressions for the topological invariants[165]. The second Chern number $C_2 \in \mathbb{Z}$ provides an invariant for the (4 + 1)-dimensional quantum Hall insulator, and, by dimensional reduction, one can derive the Chern–Simons form for strong TIs in three dimensions, which show the topological magnetoelectric effect. By further reducing the dimensionality, we obtain the class of quantum spin Hall insulators and its classification by, again, a $\mathbb{Z}_2$ invariant[5].

Excerpt of Altland–Zirnbauer symmetry classes for 2D and 3D topological insulators

Class	(2 + 1)*d*	(3 + 1)*d*	(4 + 1)*d*
A	$\mathbb{Z}$	–	–
AII	$\mathbb{Z}_2$	$\mathbb{Z}_2$	$\mathbb{Z}$

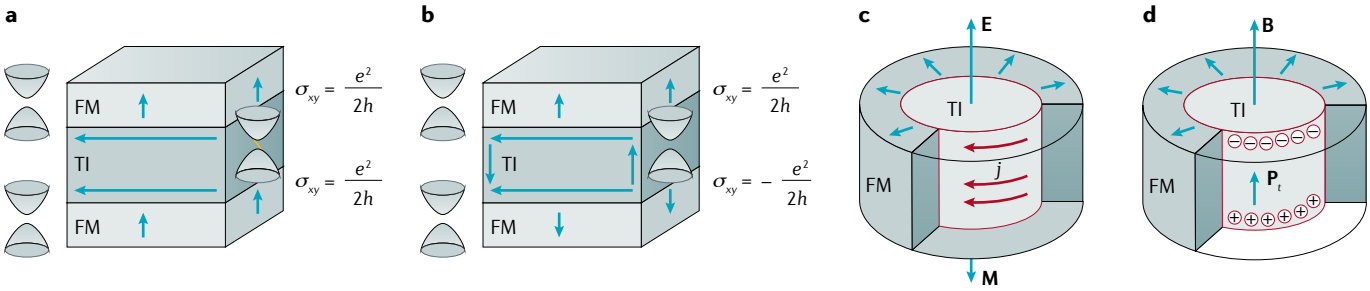

Fig. 1 | **Quantized responses in topological insulator–ferromagnet heterostructures. a** | Topological insulator (TI) cladded by ferromagnets (FMs) with parallel magnetization. Both top and bottom surface of the TI are gapped and contribute a half-quantized quantum Hall conductance σ_{xy} for a perpendicular electric field **E**. The current is carried by a chiral surface state on the side of the TI. **b** | For antiparallel configuration, the signs of the induced currents cancel and no Hall current is measured. **c** | Induced fields from the topological magnetoelectric effect when an external field is applied to a cylindrical insulator structure. A magnetization **M** is induced by an external electric field via a tangential current *j*. **d** | A polarization $\mathbf{P}_t$ builds up as a consequence of an external magnetic field **B**. Adapted with permission from REF.[5], APS.

magnetically doped TIs can aid the search for the zero quantum Hall plateau, as their topological band structure can be tuned more transparently by structural parameters[62–64].

Topological magnetoelectric effect

The topological magnetoelectric effect is a particularly intriguing phenomenon that appears when the surface of a strong TI is fully gapped, such as by an outward-pointing field[5]. Two examples are depicted in FIG. 1c,d, for a system that consists of a cylindrical TI sample wrapped by a ferromagnet with its magnetization orthogonal to the interface. Applying an electric field to the material induces a quantized current perpendicular to the normal vector of the magnetization and the field (FIG. 1c). This current then induces a magnetization antiparallel to the electric field, which is quantized in units of the fine-structure constant α,

$$\mathbf{M} = -\left(n + \frac{1}{2}\right)\alpha\mathbf{E}. \tag{11}$$

Vice versa, an external magnetic field polarizes the material along the same axis (FIG. 1d). Thus, one way to access this quantized magnetoelectric effect is through magnetic field detection. The induced polarization or magnetization can also be captured by Maxwell's equations when properly accounting for Eq. (8). BOX 2 introduces how the constitutive material relations change in the presence of the additional coupling.

The topological magnetoelectric effect contributes to the linear magnetoelectric polarizability, which can be written as[6]

$$\alpha_{ij} = \left.\frac{\partial M_j}{\partial E_i}\right|_{\mathbf{B}=0} = \left.\frac{\partial P_i}{\partial B_j}\right|_{\mathbf{E}=0} = \tilde{\alpha}_{ij} + \theta\frac{\alpha}{4\pi^2}\delta_{ij}, \tag{12}$$

where $\tilde{\alpha}_{ij}$ denotes the orbital, spin and ionic contributions, which vanish in inversion- and time-reversal-symmetric compounds[65,66]. This is particularly intriguing, as strong TIs have been shown to provide a possibility of realizing a quantized coupling of $\alpha \approx 24.3\,\mathrm{ps\,m^{-1}}$, which is an order of magnitude stronger than in typical magnetoelectric materials, such as Cr_2O_3 (REF.[67]). Not only does the coupling to the axion field allow for a quantized linear electric coupling, but structures based on wrapped 3D quantum anomalous Hall insulators have been suggested to allow for enormous magnetoelectric coupling of the order of 10^3 in natural units[55].

Quantized optical response

In optical measurements of strong TIs, such as through Kerr and Faraday set-ups, axion electrodynamics yields a quantized rotation of the field polarization axis[5]. Snell's law is unmodified in the presence of a jump in the axion field, but a non-trivial Faraday effect arises that was predicted to be observable in experiment and provides direct access to the fine-structure constant by optical means[68]. The measurement procedure[69] requires that both Kerr and Faraday rotations Θ_F should be measured while varying the external field, although, technically, it should be possible to derive the quantization from just one of these procedures. This is a generalization of a previous result that proposed a giant Kerr rotation ($\Theta_K \approx \pi/2$) in an optimized set-up[70]. In particular, the quantized Kerr and Faraday angles depend on the real part of the optical conductivity σ^{r}_{xy}, which in the long-wave limit becomes quantized. In the sample, the induced rotations can then be expressed as $\Theta_K = -\tan^{-1}(c/(2\pi\sigma^{\mathrm{r}}_{xy}))$ and $\Theta_F = \tan^{-1}(2\pi\sigma^{\mathrm{r}}_{xy}/c)$ (REFS[70,71]). To gain access to the half-quantized conductances of the top and bottom surfaces, one has to measure Kerr and Faraday rotations independently in films that are much thicker than the probing wavelength[72].

Although a well-known occurrence in high-energy physics, the proposal of an image magnetic monopole mirror charge induced by an electric charge outside the TI is a more exotic effect in the condensed-matter framework[18,73]. Electrons on the surface and induced magnetic monopoles form dyons — hypothetical particles with both electric and magnetic charge — in the static limit, and an effective field can be observed with magnetic force microscopy. This concept is explained in detail

Box 2 | Change of the constitutive relations

The topological field theory (8) predicts an additional term, $\mathcal{L}_\theta$, in the electromagnetic action of the material system that scales with the axion angle θ and the fine-structure constant α (REFS[4,5,17]),

$$\mathcal{L}_\theta = \frac{\alpha}{4\pi^2}\theta\,\mathbf{E}\cdot\mathbf{B}.$$

As an immediate consequence, this axion term leads to an extension of the Maxwell relations for all materials with an effective coupling described by

$$\begin{aligned}\nabla\cdot\mathbf{E} &= 4\pi\rho - \frac{\alpha}{\pi}(\nabla\theta)\cdot\mathbf{B}\\ \nabla\times\mathbf{B} &= \frac{4\pi}{c}\mu_0\mathbf{J} + \frac{1}{c}\frac{\partial\mathbf{E}}{\partial t}\\ &\quad + \frac{\alpha}{\pi}\left[\frac{1}{c}\mathbf{B}\left(\frac{\partial}{\partial t}\theta\right) + (\nabla\theta)\times\mathbf{E}\right],\end{aligned} \tag{13}$$

effectively altering the constitutive relations of the materials. This result can be derived both from the topological field theory, and from the microscopic topological band theory, which fixes θ in the bulk of a given material[5,54]. From Eq. (13), it is clear that only a spatial or temporal change in θ induces an observable effect.

in REF.[74], although so far there exists no experimental verification of this prediction.

Dynamical axion fields

In 2010, two studies presented the idea of topological magnetic insulators, materials that can realize the dynamic axion field by having long-range magnetic order that breaks time-reversal symmetry[17,27]. As magnetic fluctuations in these systems couple to the axion field, hybridized modes with external fields can emerge[75,76]. An example is the axion polariton, which couples the axion and the photon field and is predicted to have a dispersion relation analogous to the optical phonon polariton. One of the key differences, however, is that a gap in the spectrum of these axion polaritons can be tuned by the external magnetic field and thus can be observed in attenuated total reflection experiments[27]. No signs of this theorized quasiparticle have been observed so far, because of the lack of experimental resolution in the terahertz range and the challenge of exciting longitudinal fluctuations in existing materials[77]. At much lower frequencies, of the order of 1 Hz, the application of a slowly varying external electric field and a constant magnetic field to an axion insulator on the tip of a cantilever forces the tip of the cantilever to change its natural frequency. By microcantilever torque magnetometry, such a subtle change should be observable in experiment[27].

Axion electrodynamics in Weyl semimetals arises from the separation of band crossings, or Weyl nodes, of opposite chirality in momentum space and energy (see BOX 3). In material systems that exhibit a Fermi-surface instability, the topological bands can be gapped, and the dynamical axion field effectively couples to the phase of the emerging charge-density wave[78]. The quantum of this excitation is called a phason, and its impact on magnetotransport was detected in Ta_2Se_8I (REF.[28]).

Casimir stress
Stress that results in Casimir forces inside inhomogeneous structures.

Casimir–Lifshitz repulsion

Axion electrodynamics in topological materials has also been proposed to have observable consequences in the interactions between materials due to electromagnetic fluctuations. The Casimir–Lifshitz effect[79–82] arises from quantum fluctuations in the electromagnetic field and results in a force between two objects that are micrometres apart or closer. Although in most cases the Casimir force is attractive, repulsion (while maintaining vacuum or air between the two interacting objects) is desirable for enhanced control over friction and applications such as quantum levitation[83].

In 2011, it was proposed that both attractive and repulsive Casimir forces could be possible in a set-up involving two 3D TIs with thin magnetic layers covering each of the two interacting faces[84]. Because the constituent relations describing the electromagnetic response include extra terms due to the axion field, the authors concluded that if the magnetizations of the surface layers have opposite signs, there is a characteristic length dependent on the dielectric functions. Below this characteristic length, the Casimir–Lifshitz force is repulsive, and above it, the force is attractive, with quantum levitation being possible when the plates are separated exactly by the characteristic length. Many theoretical studies followed that examined the role of temperature[85,86], uniaxial anisotropy[85], arbitrary object shape[86], surface bandgap size[87,88], slab thickness[89] and the presence of substrates[89] on this model. Further, it was proposed that the repulsion could be enhanced by using multilayers of magnetic layer-coated TIs alternating with normal insulators[90].

Similar propositions using Chern insulators[91] or Weyl semimetals[92] instead of 3D TIs have been put forwards. Recent work, however, suggests that where repulsion is possible with the Weyl semimetal model, it is small and hard to obtain and that the Casimir–Lifshitz force is dominated instead by the metallic nature of the semimetals[93]. Although the models involving TIs seem more promising, they still require the surface Hall conductivity related to the axion field to dominate over the bulk longitudinal conductivity[94,95], and it has been argued that this makes the repulsive Casimir–Lifshitz effect unlikely to be found using topological materials[96]. Additional studies explore the Casimir stress on a TI placed between two conducting plates[97] and the repulsion between two conductors with a spatially inhomogeneous axion field between them — with a suggested realization using Weyl semimetal as the axion field medium[98]. However, these proposals do not include other material contributions such as the bulk longitudinal conductivity, which can dominate the dielectric response of these materials. All studies on the possibility of Casimir–Lifshitz repulsion in topological materials so far have been theoretical, leaving this as another avenue for experiment to explore.

Axion field in trivial materials

The effects discussed so far have the most interesting physical consequences in the regime where θ is quantized and the field coupling is maximal. In practice, however, a non-vanishing θ can exist in non-topological materials without particular symmetries present. In fact,

the well-studied magnetoelectric Cr_2O_3 and multiferroic $(Fe,Zn)_2Mo_3O_8$ may be more promising candidates than TIs for measuring the axion coupling and its contribution to the magnetoelectric polarization, as these compounds exhibit naturally gapped surface states[99,100]. The fact that the pseudoscalar contribution to the magnetoelectric tensor exists and is potentially linked to an axion field was already established in 2009, although without a microscopic expression for the coupling constant[99]. First calculations of Chern–Simons orbital magnetoelectric coupling using Wannier-based methods in real, non-topological materials (such as Cr_2O_3, $BiFeO_3$ and $GdAlO_3$) were presented in REF.[67]. It is worth mentioning here that the numerical evaluation of the axion coupling parameter remains an intricate task. Although the field theory predicts fixed values for the bulk of strong and trivial insulators, evaluating the microscopic expression, Eq. (9), for systems that lack time-reversal or inversion symmetry is not straightforward. Wannier-function-based evaluations on a finite k-space mesh reveal that Cr_2O_3 has a relatively weak coupling ($\theta \approx \pi/36$) and correctly reproduce the quantized value in Bi_2Se_3 (REF.[67]). More recently, advances have been made to calculate the axion coupling from Wannier charge centres[101]. Even though the axion contribution to the orbital magnetoelectric effect is thought to be a minor one, it should still be included in future calculations.

The preceding discussion focuses on the non-interacting case. In strongly interacting systems, quantum Hall states with fractional quantum numbers can emerge, and a topological field theory has been developed to capture these effects in 3D insulators[102]. A promising route to detect the quantization in these states is again optical spectroscopy[68].

Material realization

So far, we have only addressed the conceptual design of a topological magnetoelectric material. In this section, we aim to give an overview of real material structures that have been proposed and observed to host states that couple to axion fields FIG. 2. Here, we highlight intrinsic axion insulators and materials in which elementary excitations have axion character. Although some of the former can be derived by magnetically doping strong 3D TIs, the latter typically require the presence of excitations that gap topological semimetal states, such as a charge-density wave that is commensurate with the spacing of Weyl points on the Fermi surface[78,103]. In particular, we focus on Mn- and Cr-doped Bi_2Se_3 in heterostructures, the recently realized intrinsic topological antiferromagnets, such as $MnBi_2Te_4$ and related compounds[29,30,104–106], and the charge-density-wave Weyl semimetal Ta_2Se_8I (REFS[28,104]).

In many of the structures, experimental characterization is achieved by angle-resolved photoemission spectroscopy, which can access both bulk and surface states and probe the gap of the system with optical means, as well as by transport measurements that probe the signatures of axion electrodynamics[107].

Magnetically doped TIs

Axion electrodynamics was first proposed to emerge at interfaces between 3D TIs and trivial materials[5], and in sandwich structures with ferromagnetic materials, as visualized in FIG. 1. However, the search for an intrinsic host structure — that is, a bulk material rather than a heterostructure that breaks time-reversal symmetry and thus gaps the Dirac surface states — was guided early on by the proposal to study magnetically doped strong TIs, Bi_2Te_3, Bi_2Se_3 and Sb_2Te_3 (REFS[27]). The electronic structures of these undoped materials each exhibit a single Dirac cone on the surface, and the effective model for these materials yields values 0 and π for θ, depending on parameters. An external magnetic field applied to inversion-symmetric Bi_2Se_3 alone only breaks time-reversal symmetry, such that there cannot be a net macroscopic moment from magnetoelectricity, and inversion has to be broken by other means[34]. However, it was argued theoretically that a time-reversal-breaking perturbation can lead to axion electrodynamics in these 3D TIs. By doping the structure with 3*d*-ferromagnets,

Box 3 | **Chiral anomaly in Weyl semimetals**

The word 'anomaly' in this context refers to when a symmetry required by classical physical laws is broken in the quantum regime. The chiral anomaly, also referred to as the axial or Adler–Bell–Jackiw anomaly[166,167], is a phenomenon known in relativistic quantum field theory that arises in the axial symmetry of massless, chiral particles such as Weyl fermions. This anomaly reveals itself in the number of particles of each chirality not being separately conserved when the background gauge field is topologically non-trivial, despite this conservation being present classically[8].

Weyl semimetals are hosts to topologically protected band degeneracies[24]. These degeneracies, or nodes, disperse linearly in momentum and have an associated chirality; thus, they can be described as quasi-relativistic Weyl fermions, and Weyl semimetals are expected to exhibit the chiral anomaly when coupled to an electromagnetic field[7]. A few studies[7,8,168,169] have shown that the Hamiltonian describing the low-energy physics of a Weyl semimetal with a single pair of Weyl nodes naturally leads to the addition of an axial four-vector term to the electromagnetic action of exactly the form in equation (8), except that the axion field,

$$\theta(\mathbf{r}, t) = -2b_\mu x^\mu = 2\mathbf{b}\cdot\mathbf{r} - 2b_0 t, \tag{14}$$

is in general position-dependent (**r**) and time-dependent (t) and so remains inside the integral. Here, x is the space–time four-vector, $2\mathbf{b}$ is the momentum-space separation of the Weyl nodes, and $2b_0$ is the energetic separation in the four-vector $b = (b_0, \mathbf{b})$.

The equations of motion describing two known phenomena that can be observed in Weyl semimetals were derived by varying this action with respect to the gauge field A (REF.[168]):

$$\begin{aligned} j^\mu &= \frac{e^2}{2\pi^2} b_\nu \varepsilon^{\nu\mu\alpha\beta}\partial_\alpha A_\beta, \qquad \nu = 1, 2, 3 \\ j^\mu &= -\frac{e^2}{2\pi^2} b_0 \varepsilon^{0\mu\alpha\beta}\partial_\alpha A_\beta. \end{aligned} \tag{15}$$

Here, ε denotes the Levi–Civita symbol with space–time indices ν, μ, α, β. The first of these describes the anomalous Hall effect, caused by the breaking of the time-reversal symmetry and the separation of Weyl nodes in momentum space. The second corresponds to the chiral magnetic effect, which can result from the energetic separation of the Weyl nodes or the application of non-orthogonal electric and magnetic fields, although the former requires a dynamical non-equilibrium setting in the low-frequency (d.c.) limit[23,24,26,168]. Thus, this equation is not a complete description but a simplified representation. Although the anomalous Hall effect has already been linked to band topology and is straightforward to measure, the chiral magnetic effect is a more subtle phenomenon that has only recently been definitively captured in longitudinal magnetoresistance measurements[170]. However, both phenomena are exciting, owing to the possibility of dissipationless transport using metallic systems[25].

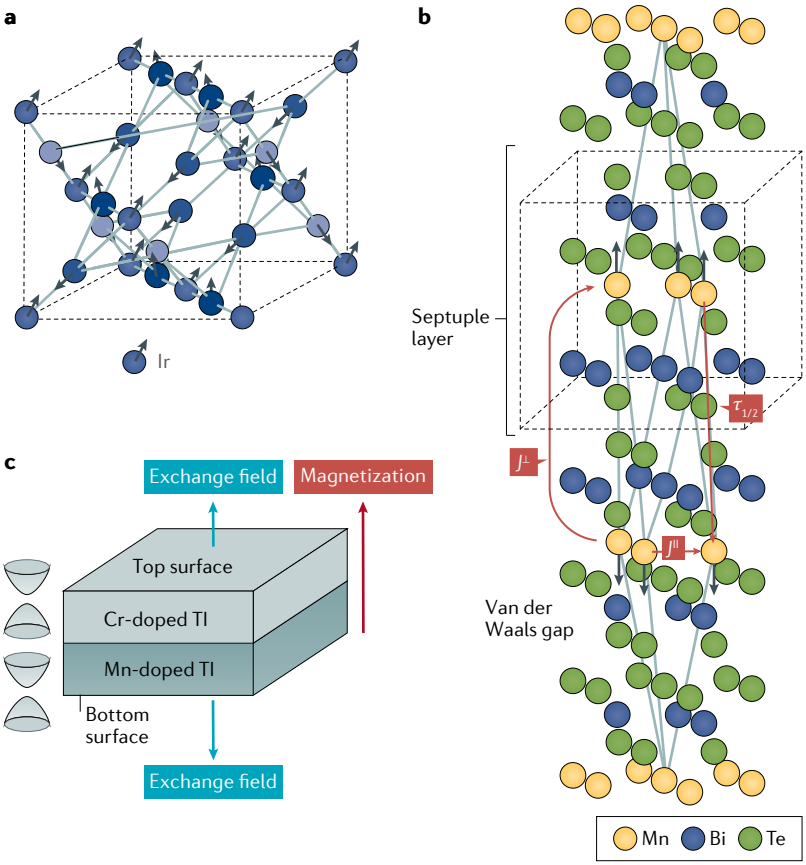

Fig. 2 | **Material systems proposed to be axion insulators. a** | Crystal structure of pyrochlore iridate $Y_2Ir_2O_7$ (Y = yttrium or lanthanide). The magnetic configuration is all-in/all-out on the network of tetrahedrons with Ir corners. **b** | Van der Waals layered $MnBi_2Te_4$ with antiferromagnetic interlayer coupling and combined lattice translation and time-reversal symmetry ($S = \tau_{1/2}\mathcal{T}$). **c** | Magnetic sandwich structure consisting of Mn- and Cr-doped strong topological insulator (TI) layers. Panel **a** adapted with permission from REF.[134], APS. Panel **b** adapted from REF.[104], Springer Nature Limited. Panel **c** adapted with permission from REF.[62], APS.

a magnetic order can be established in the material by means of a staggered Zeeman field. The axion field then couples directly to deviations of the magnetic order parameter, and collective excitations of the (anti-)ferromagnetic phase can change the otherwise constant axion field by its effective coupling $\Delta\theta \propto \Delta M_z$. This coupling of the axion field is nonlinear, except for the case of a static and uniform magnetic field, in which there is a linear coupling to the electric field.

Heterostructures of TIs

Dynamical axion states in magnetically doped TIs require long-range magnetic order[27]. In contrast to magnetically doping strong TIs in such a way that an antiferromagnetic order evolves, one can imagine staggering layers with different dopants that eventually couple antiferromagnetically across different layers. This concept arises as a natural implementation of the idea of stacking TIs[5] and was further developed in REFS[62–64], partly motivated by the lack of experimental verification of the topological magnetoelectric effect up to then. The proposals are united in their idea of using sandwich structures with different ferromagnetic capping layers. These layers, both insulating, should differ in their coercivities, making it possible to access both parallel and antiparallel magnetization configurations, analogous to what is shown in FIG. 1a,b, with one external magnetic field sweep. The zero Hall plateau obtained for antiparallel top and bottom layer magnetizations, together with fully quantized Hall plateaus in the high-field limit, yields the requirements for the existence of a topological magnetoelectric response in structures where the magnetization gap dominates the hybridization gap. Both the zero Hall plateau and the quantum anomalous Hall effect have to be measured in the same system to establish its potential to show the topological magnetoelectric response. Finite-size effects can be eliminated for large enough layers, and a gap on the dissipative side surfaces can be induced by ferromagnetic cladding in a special set-up or through quantum confinement[63]. A heterostructure with both Cr- and Mn-doped TIs (FIG. 2c) has been proposed to realize the zero Hall plateau[62]. This idea has further been extended to superstructures of these Cr- and Mn-doped TI layers to realize electrodynamic axion coupling that was previously proposed for antiferromagnetic TIs[27,64].

Antiferromagnetic TIs

It was not until late 2018 that a stoichiometric material compound, $MnBi_2Te_4$, was predicted and experimentally confirmed as an antiferromagnetic TI[104]. This study on the topological properties of $MnBi_2Te_4$ (FIG. 2b) was soon followed by a large amount of theoretical and experimental work[29,105,108–116]. $MnBi_2Te_4$ is a layered ternary tetradymite compound first synthesized as a powder in 2013 (REFS[104,117]). The crystal structure of $MnBi_2Te_4$ is shown in FIG. 2b and comprises blocks of septuple layers along the (0001)-direction in the trigonal structure of space group $R\bar{3}m$ (no. 166). The layers are bound by van der Waals forces, and Mn moments couple antiferromagnetically across layers. Within the Mn layers, the magnetic moments show ferromagnetic order, such that an operation, S, that combines a half-layer translation $\tau_{1/2}$ and time reversal $\mathcal{T}$ such that $S = \mathcal{T}\tau_{1/2}$ realizes the necessary symmetry to classify the material as a $\mathbb{Z}_2 = 1$ antiferromagnetic insulator[17]. Both the bulk and the surface states were first reported to be gapped, with values of 220 meV and 88 meV, respectively[104]. The Néel temperature of the compound was calculated to be about 25 K, below which the topological magnetoelectric effect should be observable. Subsequent experimental investigations noted the difficulty of accessing gapped surface states, in part owing to the strongly n-type doping and observed gapless Dirac cones in angle-resolved photoemission studies[115,118,119]. It was later proposed to substitute Sb in the position of Bi to tailor its Fermi level to within the bulk and surface gap[110]. Irrespective of this controversy, $MnBi_2Te_4$ was predicted to have a rich phase diagram in all of its magnetic phases across 2D and 3D samples[120] and, further, to exhibit second-harmonic generation and a shift current from infrared photons that is two orders of magnitude above typical shift currents obtained in non-topological ferroelectrics[121]. Samples can be grown by molecular-beam epitaxy or by a self-flux method to obtain single crystals[105,109]. One of the main challenges

Shift current
Second-order optical effect that results in a d.c. current from incident monochromatic light.

during the growing procedure is the precise temperature control required[122]. In measurements, one has to finely tune the chemical potential into the insulating surface gap, and finite-thickness effects have to be eliminated[30].

A number of variations of $MnBi_2Te_4$ have been proposed as candidate materials for axion insulators and to realize dynamic axion fields. Among them are $Mn_2Bi_2Te_5$, which realizes different surface states from $MnBi_2Te_4$ (REF.[120]), and $MnBi_{2n}Te_{3n+1}$, which, depending on the surface termination, was shown to exhibit different topological states[106]. $Mn_2Bi_2Te_5$ and $Eu_2Bi_2Te_5$ break both inversion and time-reversal symmetry but preserve their product and consequently show a non-quantized θ (REFS[77,123]). However, unlike in $MnBi_2Te_4$, non-static axion states can be realized through antiferromagnetic resonance, opening a path to observe dynamic axion effects[77]. To realize specific stable magnetic configurations, several studies suggest heterostructures that contain $MnBi_2Te_4$ and related compounds[124–127]. In particular, the coercive fields of these structures are easier to control — both in and by external fields — than doped TIs[124].

An intrinsic antiferromagnetic insulator state has also been proposed to arise in $EuIn_2As_2$, which has a hexagonal crystal structure with the space group $P6_3/mmc$ (no. 194)[128]. This material shows a smaller bulk insulating gap and a lower Néel temperature than $MnBi_2Te_4$ but is a candidate material to realize the axion insulator state in its two antiferromagnetic phases as well as a higher-order TI state. For antiferromagnetic order along the crystallographic *c*-axis, one can construct a cylinder with all surfaces being gapped. An effective 1D behaviour emerges in the hinges between surface planes. A number of studies have followed this proposal and identified the in-plane magnetic configuration as the ground state in $EuIn_2As_2$ (REFS[129,130]). More recently, $EuSn_2As_2$ (REF.[116]) and $EuSn_2P_2$ (REF.[131]) have been shown to exhibit comparable properties, extending the list of synthesized and characterized antiferromagnetic TIs even further.

To aid measurements of the zero Hall plateau and quantum anomalous Hall effect, a stacking similar to the proposed sandwich structures depicted in FIG. 2 has been suggested but with antiferromagnetic $MnBi_2Se_4$ on one side of the strong TI[132]. In that way, the expected response depends only on the magnetization of one ferromagnetic layer.

Charge-density-wave materials

In Weyl semimetals, which host ungapped, chiral topological states in the bulk of the material, a charge-density wave can destroy the intrinsic chiral symmetry and convert the otherwise conducting material into a topologically non-trivial insulator[78,133]. The phase fluctuations of this induced density wave couple directly to an axion-like field. This phase preserves time-reversal symmetry, such that no anomalous Hall effect is expected. We elaborate on the details of this mechanism and comment on recent experimental efforts in Ta_2Se_8I in the next section[28].

Other material compounds

Several other materials have been predicted to be axion insulators but have so far eluded experimental verification as such.

Density-functional calculations with self-interaction-corrected local spin density approximation show that the ground state of pyrochlore iridates (such as $Y_2Ir_2O_7$; FIG. 2a) is a 3D semimetal with Fermi arc surface states and non-collinear magnetic order[134]. On changing the Coulomb interaction parameter *U*, the material exhibits several phases, among them the axion insulator state, protected by inversion symmetry, and a Mott insulator state. This was further confirmed in a theoretical study in a wider range of compounds[135]. By manipulating the surface termination and the magnetic structure in a model system describing the pyrochlore iridate lattice, a range of accessible topological states have been found, including phases of higher-order topology[56]. The axion insulator state in these compounds is stabilized by inversion symmetry. In a similar spirit, it was later predicted that osmium compounds such as $CaOs_2O_4$ and $SrOs_2O_4$ can be stabilized in the geometrically frustrated spinel crystal structure and show an equally colourful phase diagram when varying *U*, again including the axion insulator state[134,136,137]. So far, both structures have eluded experimental verification of the axion phase.

With a Néel temperature of 9 K, GdPtBi was proposed in 2010 as a possible candidate axion insulator[17], but it was verified to be a semimetal with antiferromagnetic order in subsequent experimental studies[138–140]. However, recent experimental work suggests that a negative magnetothermal resistivity in GdPtBi may be a signature of the mixed axial–gravitational anomaly[141].

Experimental realizations

The theoretical prediction of a half-quantized quantum Hall effect quickly stimulated experimental efforts to observe this effect. The topological magnetoelectric effect promises unprecedented coupling strengths even in inversion-symmetric or time-reversal-invariant materials. To establish a platform for the axion insulator state, one of the main measurement objectives is to observe the zero Hall plateau along with the quantum anomalous Hall effect in typical six-terminal devices and in a material where the magnetization gap dominates the hybridization gap[32,62] (FIG. 3a,b). As the individual surfaces are not individually accessible in traditional transport experiments, measurement of the magnetoelectric effect, which manifests itself as a bulk property, becomes a main objective. Optical measurements can provide a direct and non-contact route to the quantized response of both bulk and surface states. The main experimental challenge remains in the fact that these states need to be sufficiently gapped.

Optical measurements

Several groups have presented direct measurements of the Kerr rotation in strong 3D TIs using either high external magnetic fields or magnetic impurities to break time-reversal symmetry[34,36,37]. In one of these recent experiments, Bi_2Se_3 samples from molecular-beam epitaxy were measured in a terahertz magneto-optical Faraday set-up, and a half-integer quantization index was observed[34] (FIG. 3c,d. This work claims direct evidence for the optical response altered by the presence of the

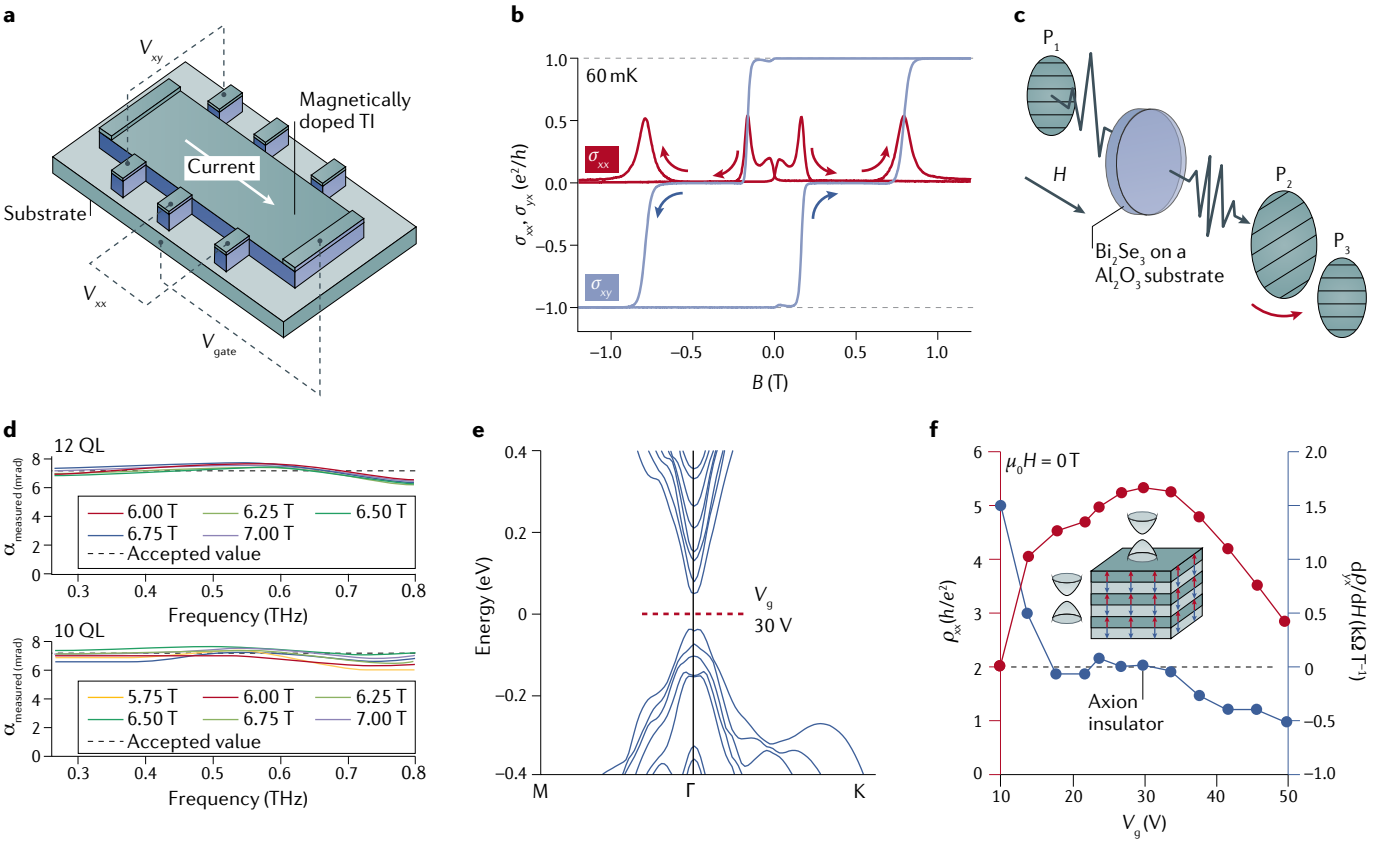

Fig. 3 | **Experimental set-ups to access topological responses. a** | Six-terminal transport device used for Hall measurements. **b** | Temperature-dependent observation of the zero Hall plateau and quantum anomalous Hall effect at fixed gate voltage in sandwich structure of ferromagnetic Cr-doped $(Bi,Sb)_2Te_3$, non-magnetic $(Bi,Sb)_2Te_3$ and ferromagnetic V-doped $(Bi,Sb)_2Te$. **c** | Terahertz polarization measurement set-up for Bi_2Se_3 in high external magnetic fields. P_1, P_2, P_3, polarizers. **d** | Measurement results for the fine-structure constants extrapolated from the induced rotation in samples of different thickness (number of quintuple layers (QLs)) and for varying external fields. **e** | Bulk band structure of $MnBi_2Te_4$ with antiferromagnetic ordering and chemical potential with gate voltage 30 V. **f** | Longitudinal resistivity and change in the Hall resistivity around zero field. TI, topological insulator. Panel **b** adapted with permission from REF.[144], AAAS. Panels **c** and **d** adapted with permission from REF.[34], AAAS. Panels **e** and **f** adapted from REF.[147], Springer Nature Limited.

axion term, using time-domain terahertz spectroscopy[34]. The experiment overcame a number of technical challenges, as the probe frequency has to be much lower than the Landau-level splitting induced by the external magnetic field that gaps the surface states. As metallic gates would induce their own Faraday rotation, bulk doping has to be accurately controlled (to eliminate the need for gating), which further complicates direct measurement of the quantized response. By measuring the induced change in polarization of both transmitted and reflected fields, the fine-structure constant was extracted with an accuracy of 0.5%. This result does not depend on the particular substrate, as it does in optical measurements of 2D electron gases or graphene in the quantum Hall regime[142,143]. Thus, the direct observation of the quantized Faraday response paves the way towards a definition based purely on topological invariants in a solid-state system for three fundamental physical constants (e, h and c)[34,69].

Comparable results were presented in strained HgTe 3D TI structures[36,37]. Near-quantization was achieved in REF.[37] without the need for any external field. In REF.[36], high magnetic fields and semi-transparent gates were used such that interface doping was not necessary to reduce carrier concentration as in REF.[34]. Control of the Fermi level by gel gating was achieved, which can provide access to both semiclassical and quantized responses in terahertz spectroscopy[35].

It is worth noting that whereas a quantized Faraday rotation was reported in the aforementioned experiments, the observation of a half-quantized surface Hall effect, or equivalently the topological magnetoelectric effect, has not been achieved yet. Although the structures probed in these recent experiments do not qualify as axion insulators per se, and their response can be explained in terms of the quantum Faraday effect, it can also be derived from axion electrodynamics with appropriate boundary conditions. Both effects can in principle be realized in antiferromagnetic or ferromagnetically doped TIs as well[54,72].

The proposed axion polariton has so far eluded observation through optical measurements. Together with the proposal of a cantilever torque magnetometry measurement, the two experiments of dynamical properties proposed in REF.[27] can be addressed in future experiments, given clean and large enough crystal samples for both intrinsic and synthetic material structures.

Transport measurements

TI heterostructures. The axion insulator state leads to the topological magnetoelectric effect. To realize this state in a 3D heterostructure, the surfaces need to be gapped and the bulk needs to quantize such that $\theta = \pi$ (REFS[33,62]). As shown in FIG. 1a,b, by switching the magnetization configuration in such a layered structure, one can observe both the quantum anomalous Hall regime and the zero Hall plateau, which provides the motivation for further investigation[63]. Two of the first studies to realize the axion insulator state accessed by magnetotransport measurements use molecular-beam epitaxy to grow trilayers $(Bi,Sb)_2Te_3$ with V-doping of the top and Cr-doping of the bottom layer[33,144]. For the parallel magnetization configuration, the quantum anomalous Hall effect is observed, whereas in the antiparallel orientation, the existence of a zero Hall plateau was verified. These studies move closer to measuring the axion insulator state than previous work that identified plateaus of zero Hall conductance[32,145], but, in the regime where the hybridization gap dominates the magnetization gap, the identification of an antiparallel magnetization configuration remains unclear[146].

Antiferromagnetic TIs. Antiferromagnetic TIs provide a platform to measure the quantum anomalous Hall effect in stoichiometric compounds. Most of the early studies on $MnBi_2Te_4$ focused on characterization of bulk and surface states by angle-resolved photoemission[104,106,118,120,122] and exploring its rich magnetic and topological phase diagram. More recently, an axion-to-Chern-insulator transition was observed at moderate magnetic fields in samples with an even number of layers. This result is shown in FIG. 3e,f, together with the dispersion of the $MnBi_2Te_4$ surface states[147]. In $MnBi_2Te_4$ flakes with an odd number of layers, where the surface layers show antiparallel magnetization alignment, the quantum anomalous Hall effect was observed at zero field, and the Hall resistance exhibited finite jumps when individual magnetic layers switched due to an external field[111].

Charge-density waves. The first measurement of a dynamic axion realization was reported in 2019 and used transport measurements in quasi-1D Ta_2Se_8I (REF.[28]). This compound is a Weyl semimetal at room temperature and opens a bulk gap at lower temperatures owing to the formation of a charge-density wave[148]. A peculiar detail in this system is that the charge-density-wave nesting vector coincides with the vectors connecting the 24 Fermi-surface Weyl points. The phase of this charge-density wave can be identified as a contribution to the axion field, and the phason is the axionic mode. The effective action describing the electrodynamics in this compound shows analogies to that of the pion–photon coupling in high-energy physics[78]. Ta_2Se_8I further shows the highest net chiral charge (the sum of Weyl node chiralities below the Fermi level) reported in a Weyl semimetal so far, up to +16. The effect of the axion mode is visible in magnetotransport measurements. By applying a magnetic field parallel to the depinning electric field that permits the charge-density wave to slide, the axion coupling to the phase of the charge-density wave is established, and this coupling yields a positive contribution to the magnetoconductance. The contribution scales with the applied magnetic field and allows identification of the axion character of the phason. In FIG. 4, we show the unit cell of Ta_2Se_8I, the gapping mechanism mediated by the formation of a charge-density wave, and the identifying measurement of the magnetoresistance. This mechanism should be observable in any Fermi-surface Weyl semimetal that exhibits a charge-density wave with coupling commensurate to the spacing of the Weyl points in momentum space. It is worth noting that whether or not Ta_2Se_8I qualifies as an axion insulator is a subject of ongoing debate[133]. It does, however, realize a dynamical axion field through the chiral anomaly and its charge-density wave. Whether it shows non-trivial magnetoelectric response needs to be established by further studies.

Nesting vector
Vector connecting pockets of the Fermi surface, typically related to the formation of a density wave.

Applications

In addition to the striking quantized responses emerging from the axion coupling and the possibility of constructing structures with enormous linear magnetoelectric coefficients, several practical applications have recently been proposed for axion insulators. Among them, and certainly one of the most intriguing possibilities, is the idea of using antiferromagnetic TIs and their axion polaritons to detect the dark-matter axion by low-noise terahertz techniques[149]. Dark-matter axions are hypothetical particles that could account for most or all of the dark matter in the Universe. One proposal is a device made of Fe-doped Bi_2Se_3, in which dark-matter axions can effectively drive the condensed-matter axion polariton by electromagnetic coupling. As the axion polariton dispersion in the antiferromagnetic TI is sensitive to the external magnetic field, axion masses between 0.7 meV and 3.5 meV can be scanned, which would fill a gap in the range of detectable fundamental axion energies[150]. This theoretical proposal assumes relatively large crystals (1 cm^3 of antiferromagnetically doped $(Bi_{1-x}Fe_x)_2Se_3$), which need to exhibit gapped bandstructures at both bulk and surface, and so the implementation of such a detector provides ample challenges to device design and material synthesis.

Axion electrodynamics can also contribute to the asymmetry of the dielectric tensor of a Weyl semimetal via the chiral anomaly (BOX 3), given the emergent axion field's spatiotemporal nature. If a Weyl semimetal has broken time-reversal symmetry and nodes separated in momentum space, its surface plasmon polariton modes can be strongly non-reciprocal[151]. Thus, these materials provide an efficient way to construct non-reciprocal thermal emitters. A new method to control thermal radiation is by exploiting the temperature-tunable non-reciprocity of radiation in magnetic Weyl semimetals[152]. This technique makes it possible generally to overcome accepted photovoltaic performance limits[153]. The proposal assumes a perfect Weyl semimetal with the minimum number of two Weyl nodes at the Fermi level. Such states have already been observed in $EuCd_2As_2$, such that future measurements could be used to assess the feasibility of such a device[154].

More exotic proposals range from superconducting phases that can couple to the topological axion field[155] to the realization of Majorana fermions at the interface

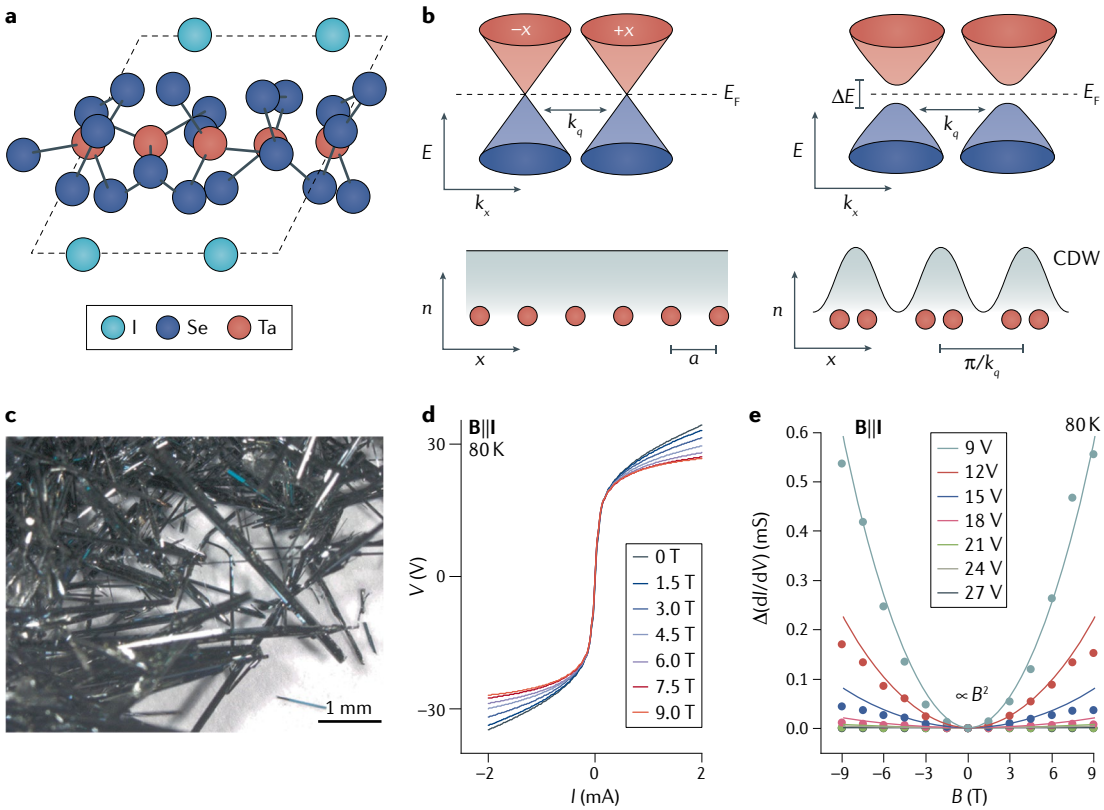

Fig. 4 | **Signature of axionic charge-density wave in Ta_2Se_8I. a** | Crystal structure of Ta_2Se_8I with quasi-1D character. **b** | Simplified picture of a charge-density wave (CDW) with a wave vector k_q commensurate with the spacing of the Weyl points, which gaps the states at the Fermi level E_F. The CDW appears in the direction of the Ta-chain (*x*). **c** | Grown crystals of Ta_2Se_8I. **d** | Resulting voltage–current (*V*–*I*) curve for magnetic fields parallel to depinning field from sample shown in panel **c**. **e** | Quadratic dependence of the magnetoconductance on the external field for various voltages. Adapted from REF.[28], Springer Nature Limited.

between quantum anomalous Hall materials, together with its prospects for topological quantum computing[15,156,157].

Outlook

Just as quantum Hall insulators were observed within a decade after the initial theoretical prediction, axion states are now accessible in a number of condensed-matter systems, pushing theory, material synthesis and experimental characterization to their limits.

Although the axion particle in high-energy physics still eludes observation, its low-energy condensed-matter counterpart can be realized in various ways. Part of this success comes from the topological field theory of the axion insulator allowing for a classification of 3D insulators with and without time-reversal symmetry. Apart from its quantized coupling to an external field, the axion parameter can take continuous values in semimetallic and non-symmetric systems and thus contributes significantly to the linear magnetoelectric response. The magnetoelectric coupling by the axion term arises, although with lower magnitude, even in topologically trivial materials, such that its calculation is necessary to accurately predict their response.

So far, experimental discoveries have largely followed theoretical predictions in this field, in contrast with developments in the field of superconductivity. Excitingly, first principles predictions have fuelled the demand for clean crystal samples and ultra-high-precision measurements. On the other hand, calculations of the topological band structure and their response will be put to a test in highly correlated materials that undergo phase transitions, where computational approaches based on the single-particle picture fail.

Topological antiferromagnets that have sizable gaps and transition temperatures at elevated temperatures are yet to be realized. A direct observation of the topological magnetoelectric effect, for example, in optical experiments that are sensitive to a single surface, or realizations of the dynamical axion field in antiferromagnetic TIs is still missing. Bringing about the first technologically relevant application of a 3D TI that harnesses giant quantized responses, this is a challenge that would be overcome by further material searches, synthesis and careful experiments[158]. Many practical applications in quantum information science and spintronics can be enabled from the transport behaviour exhibited[13,15,159], and fundamental science can also greatly benefit from the prospects of detecting the hypothetical dark-matter axion through realization of a new type of condensed-matter detector. The detection of such a dark axion by means of the condensed-matter counterpart would elegantly close a circle.

Published online: 30 September 2020

1. Svrcek, P. & Witten, E. Axions in string theory. *J. High Energy Phys.* **2006**, 051–051 (2006).
2. Peccei, R. D. & Quinn, H. R. *CP* conservation in the presence of pseudoparticles. *Phys. Rev. Lett.* **38**, 1440–1443 (1977).
3. Preskill, J., Wise, M. B. & Wilczek, F. Cosmology of the invisible axion. *Phys. Lett. B* **120**, 127–132 (1983).
4. Wilczek, F. Two applications of axion electrodynamics. *Phys. Rev. Lett.* **58**, 1799–1802 (1987).
5. Qi, X.-L., Hughes, T. L. & Zhang, S.-C. Topological field theory of time-reversal invariant insulators. *Phys. Rev. B* **78**, 195424 (2008).
Unified topological Chern–Simons field theory in phase space for time-reversal invariant insulators.
6. Essin, A. M., Moore, J. E. & Vanderbilt, D. Magnetoelectric polarizability and axion electrodynamics in crystalline insulators. *Phys. Rev. Lett.* **102**, 146805 (2009).
7. Grushin, A. G. Consequences of a condensed matter realization of Lorentz-violating QED in Weyl semi-metals. *Phys. Rev. D* **86**, 045001 (2012).
8. Zyuzin, A. A. & Burkov, A. A. Topological response in Weyl semimetals and the chiral anomaly. *Phys. Rev. B* **86**, 115133 (2012).
9. Hasan, M. Z. & Kane, C. L. Colloquium: Topological insulators. *Rev. Mod. Phys.* **82**, 3045–3067 (2010).
10. Qi, X.-L. & Zhang, S.-C. Topological insulators and superconductors. *Rev. Mod. Phys.* **83**, 1057–1110 (2011).
11. Vergniory, M. et al. A complete catalogue of high-quality topological materials. *Nature* **566**, 480–485 (2019).
12. Ando, Y. Topological insulator materials. *J. Phys. Soc. Jpn* **82**, 102001 (2013).
13. Šmejkal, L., Mokrousov, Y., Yan, B. & MacDonald, A. H. Topological antiferromagnetic spintronics. *Nat. Phys.* **14**, 242 (2018).
14. Moore, J. E. & Balents, L. Topological invariants of time-reversal-invariant band structures. *Phys. Rev. B* **75**, 121306 (2007).
15. Stern, A. & Lindner, N. H. Topological quantum computation — from basic concepts to first experiments. *Science* **339**, 1179–1184 (2013).
16. Kane, C. L. & Mele, E. J. Z_2 topological order and the quantum spin Hall effect. *Phys. Rev. Lett.* **95**, 146802 (2005).
17. Mong, R. S. K., Essin, A. M. & Moore, J. E. Antiferromagnetic topological insulators. *Phys. Rev. B* **81**, 245209 (2010).
18. Zirnstein, H.-G. & Rosenow, B. Topological magnetoelectric effect: nonlinear time-reversal-symmetric response, Witten effect, and half-integer quantum Hall effect. *Phys. Stat. Solidi B* **257**, 1900698 (2020).
19. Essin, A. M., Turner, A. M., Moore, J. E. & Vanderbilt, D. Orbital magnetoelectric coupling in band insulators. *Phys. Rev. B* **81**, 205104 (2010).
20. Turner, A. M., Zhang, Y., Mong, R. S. K. & Vishwanath, A. Quantized response and topology of magnetic insulators with inversion symmetry. *Phys. Rev. B* **85**, 165120 (2012).
21. Wilczek, F. Particle physics and condensed matter: the saga continues. *Phys. Scr.* **T168**, 014003 (2016).
22. Nielsen, H. & Ninomiya, M. The Adler–Bell–Jackiw anomaly and Weyl fermions in a crystal. *Phys. Lett. B* **130**, 389–396 (1983).
23. Vazifeh, M. M. & Franz, M. Electromagnetic response of Weyl semimetals. *Phys. Rev. Lett.* **111**, 027201 (2013).
24. Armitage, N. P., Mele, E. J. & Vishwanath, A. Weyl and Dirac semimetals in three-dimensional solids. *Rev. Mod. Phys.* **90**, 015001 (2018).
25. Ilan, R., Grushin, A. G. & Pikulin, D. I. Pseudo-electromagnetic fields in 3D topological semimetals. *Nat. Rev. Phys.* **2**, 29–41 (2019).
26. Burkov, A. A. Weyl metals. *Annu. Rev. Condens. Matter Phys* **9**, 359–378 (2018).
27. Li, R., Wang, J., Qi, X.-L. & Zhang, S.-C. Dynamical axion field in topological magnetic insulators. *Nat. Phys.* **6**, 284–288 (2010).
Theory and predictions on the dynamical axion field in magnetically doped TIs.
28. Gooth, J. et al. Axionic charge-density wave in the Weyl semimetal $(TaSe_4)_2I$. *Nature* **575**, 315 (2019).
Magnetoresistance experiments in axionic charge-density-wave material Ta_2Se_8I.
29. Liu, C. et al. Robust axion insulator and Chern insulator phases in a two-dimensional antiferromagnetic topological insulator. *Nat. Mater.* **19**, 522–527 (2020).
30. Zhang, D. et al. Topological axion states in magnetic insulator $MnBi_2Te_4$ with the quantized magnetoelectric effect. *Phys. Rev. Lett.* **122**, 206401 (2019).
31. Feng, Y. et al. Observation of the zero Hall plateau in a quantum anomalous Hall insulator. *Phys. Rev. Lett.* **115**, 126801 (2015).
32. Mogi, M. et al. A magnetic heterostructure of topological insulators as a candidate for an axion insulator. *Nat. Mater.* **16**, 516–521 (2017).
33. Xiao, D. et al. Realization of the axion insulator state in quantum anomalous Hall sandwich heterostructures. *Phys. Rev. Lett.* **120**, 056801 (2018).
34. Wu, L. et al. Quantized Faraday and Kerr rotation and axion electrodynamics of a 3D topological insulator. *Science* **354**, 1124–1127 (2016).
35. Mondal, M. et al. Electric field modulated topological magnetoelectric effect in Bi_2Se_3. *Phys. Rev. B* **98**, 121106 (2018).
36. Dziom, V. et al. Observation of the universal magnetoelectric effect in a 3D topological insulator. *Nat. Commun.* **8**, 15197 (2017).
37. Okada, K. N. et al. Terahertz spectroscopy on Faraday and Kerr rotations in a quantum anomalous Hall state. *Nat. Commun.* **7**, 12245 (2016).
38. Peccei, R. D. & Quinn, H. R. Constraints imposed by *CP* conservation in the presence of pseudoparticles. *Phys. Rev. D* **16**, 1791–1797 (1977).
39. Klitzing, K. V., Dorda, G. & Pepper, M. New method for high-accuracy determination of the fine-structure constant based on quantized Hall resistance. *Phys. Rev. Lett.* **45**, 494–497 (1980).
40. Thouless, D. J., Kohmoto, M., Nightingale, M. P. & den Nijs, M. Quantized Hall conductance in a two-dimensional periodic potential. *Phys. Rev. Lett.* **49**, 405 (1982).
41. Bernevig, B. A., Hughes, T. L. & Zhang, S.-C. Quantum spin Hall effect and topological phase transition in HgTe quantum wells. *Science* **314**, 1757–1761 (2006).
42. König, M. et al. Quantum spin Hall insulator state in HgTe quantum wells. *Science* **318**, 766–770 (2007).
43. Mehta, M. L. *Random Matrices* (Elsevier, 2004).
44. Fu, L. & Kane, C. L. Time reversal polarization and a Z_2 adiabatic spin pump. *Phys. Rev. B* **74**, 195312 (2006).
45. Fu, L. & Kane, C. L. Topological insulators with inversion symmetry. *Phys. Rev. B* **76**, 045302 (2007).
46. Soluyanov, A. A. & Vanderbilt, D. Computing topological invariants without inversion symmetry. *Phys. Rev. B* **83**, 235401 (2011).
47. Yu, R., Qi, X. L., Bernevig, A., Fang, Z. & Dai, X. Equivalent expression of Z_2 topological invariant for band insulators using the non-Abelian Berry connection. *Phys. Rev. B* **84**, 075119 (2011).
48. Ringel, Z., Kraus, Y. E. & Stern, A. Strong side of weak topological insulators. *Phys. Rev. B* **86**, 045102 (2012).
49. Mong, R. S. K., Bardarson, J. H. & Moore, J. E. Quantum transport and two-parameter scaling at the surface of a weak topological insulator. *Phys. Rev. Lett.* **108**, 076804 (2012).
50. Hsieh, D. et al. A topological Dirac insulator in a quantum spin Hall phase. *Nature* **452**, 970–974 (2008).
51. Xia, Y. et al. Observation of a large-gap topological-insulator class with a single Dirac cone on the surface. *Nat. Phys.* **5**, 398–402 (2009).
52. Bansil, A., Lin, H. & Das, T. Colloquium: Topological band theory. *Rev. Mod. Phys.* **88**, 021004 (2016).
53. Malashevich, A., Souza, I., Coh, S. & Vanderbilt, D. Theory of orbital magnetoelectric response. *New Journal of Physics* **12**, 053032 (2010).
54. Armitage, N. P. & Wu, L. On the matter of topological insulators as magnetoelectrics. *SciPost Phys.* **6**, 46 (2019).
Review of magnetoelectric responses and their connection to the effective polarization.
55. Vanderbilt, D. *Berry Phases in Electronic Structure Theory: Electric Polarization, Orbital Magnetization and Topological Insulators* (Cambridge Univ. Press, 2018).
56. Varnava, N. & Vanderbilt, D. Surfaces of axion insulators. *Phys. Rev. B* **98**, 245117 (2018).
57. Wang, Z., Qi, X.-L. & Zhang, S.-C. Equivalent topological invariants of topological insulators. *New J. Phys.* **12**, 065007 (2010).
58. Fang, C., Gilbert, M. J. & Bernevig, B. A. Topological insulators with commensurate antiferromagnetism. *Phys. Rev. B* **88**, 085406 (2013).
59. Tokura, Y., Yasuda, K. & Tsukazaki, A. Magnetic topological insulators. *Nat. Rev. Phys.* **1**, 126–143 (2019).
60. Bernevig, B. A. & Hughes, T. L. *Topological Insulators and Topological Superconductors* (Princeton Univ. Press, 2013).
61. Nomura, K. & Nagaosa, N. Surface-quantized anomalous Hall current and the magnetoelectric effect in magnetically disordered topological insulators. *Phys. Rev. Lett.* **106**, 166802 (2011).
62. Morimoto, T., Furusaki, A. & Nagaosa, N. Topological magnetoelectric effects in thin films of topological insulators. *Phys. Rev. B* **92**, 085113 (2015).
63. Wang, J., Lian, B., Qi, X.-L. & Zhang, S.-C. Quantized topological magnetoelectric effect of the zero-plateau quantum anomalous Hall state. *Phys. Rev. B* **92**, 081107 (2015).
64. Wang, J., Lian, B. & Zhang, S.-C. Dynamical axion field in a magnetic topological insulator superlattice. *Phys. Rev. B* **93**, 045115 (2016).
65. Rivera, J.-P. A short review of the magnetoelectric effect and related experimental techniques on single phase (multi-) ferroics. *Eur. Phys. J. B* **71**, 299 (2009).
66. fiebig, M. & Spaldin, N. A. Current trends of the magnetoelectric effect. *Eur. Phys. J. B* **71**, 293 (2009).
67. Coh, S., Vanderbilt, D., Malashevich, A. & Souza, I. Chern–Simons orbital magnetoelectric coupling in generic insulators. *Phys. Rev. B* **83**, 085108 (2011).
Numerical calculation of the axion field in topologically trivial and non-trivial materials, based on maximally localized Wannier functions.
68. Karch, A. Electric–magnetic duality and topological insulators. *Phys. Rev. Lett.* **103**, 171601 (2009).
69. Maciejko, J., Qi, X.-L., Drew, H. D. & Zhang, S.-C. Topological quantization in units of the fine structure constant. *Phys. Rev. Lett.* **105**, 166803 (2010).
70. Tse, W.-K. & MacDonald, A. H. Giant magneto-optical Kerr effect and universal Faraday effect in thin-film topological insulators. *Phys. Rev. Lett.* **105**, 057401 (2010).
71. Feng, W. et al. Topological magneto-optical effects and their quantization in noncoplanar antiferromagnets. *Nat. Commun.* **11**, 1–9 (2020).
72. Beenakker, C. Topological magnetoelectric effect versus quantum Faraday effect. *J. Club Condens. Matter Phys*. https://doi.org/10.36471/JCCM_April_2016_01 (2016).
73. Qi, X.-L., Li, R., Zang, J. & Zhang, S.-C. Inducing a magnetic monopole with topological surface states. *Science* **323**, 1184–1187 (2009).
74. König, E. J. et al. Half-integer quantum Hall effect of disordered Dirac fermions at a topological insulator surface. *Phys. Rev. B* **90**, 165435 (2014).
75. Taguchi, K. et al. Electromagnetic effects induced by a time-dependent axion field. *Phys. Rev. B* **97**, 214409 (2018).
76. Ooguri, H. & Oshikawa, M. Instability in magnetic materials with a dynamical axion field. *Phys. Rev. Lett.* **108**, 161803 (2012).
77. Zhang, J. et al. Large dynamical axion field in topological antiferromagnetic insulator $Mn_2Bi_2Te_5$. *Chin. Phys. Lett.* **37**, 077304 (2020).
78. Wang, Z. & Zhang, S.-C. Chiral anomaly, charge density waves, and axion strings from Weyl semimetals. *Phys. Rev. B* **87**, 161107 (2013).
79. Casimir, H. B. G. On the attraction between two perfectly conducting plates. *Proc. K. Ned. Akad. Wet.* **51**, 793 (1948).
80. Lifshitz, E. M. et al. in *Perspectives in Theoretical Physics* 329–349 (Elsevier, 1992).
81. Dzyaloshinskii, I. E., Lifshitz, E. M. & Pitaevskii, L. P. The general theory of van der Waals forces. *Adv. Phys.* **10**, 165–209 (1961).
82. Rivera, N., flick, J. & Narang, P. Variational theory of nonrelativistic quantum electrodynamics. *Phys. Rev. Lett.* **122**, 193603 (2019).
83. Capasso, F., Munday, J. N., Iannuzzi, D. & Chan, H. B. Casimir forces and quantum electrodynamical torques: physics and nanomechanics. *IEEE J. Sel. Top. Quantum Electron.* **13**, 400–414 (2007).
84. Grushin, A. G. & Cortijo, A. Tunable Casimir repulsion with three-dimensional topological insulators. *Phys. Rev. Lett.* **106**, 020403 (2011).
85. Grushin, A. G., Rodriguez-Lopez, P. & Cortijo, A. Effect of finite temperature and uniaxial anisotropy on the Casimir effect with three-dimensional topological insulators. *Phys. Rev. B* **84**, 045119 (2011).
86. Rodriguez-Lopez, P. Casimir repulsion between topological insulators in the diluted regime. *Phys. Rev. B* **84**, 165409 (2011).

87. Chen, L. & Wan, S. Casimir interaction between topological insulators with finite surface band gap. *Phys. Rev. B* **84**, 075149 (2011).
88. Chen, L. & Wan, S. Critical surface band gap of repulsive Casimir interaction between three-dimensional topological insulators at finite temperature. *Phys. Rev. B* **85**, 115102 (2012).
89. Nie, W., Zeng, R., Lan, Y. & Zhu, S. Casimir force between topological insulator slabs. *Phys. Rev. B* **88**, 085421 (2013).
90. Zeng, R. et al. Enhancing Casimir repulsion via topological insulator multilayers. *Phys. Lett. A* **380**, 2861–2869 (2016).
91. Rodriguez-Lopez, P. & Grushin, A. G. Repulsive Casimir effect with Chern insulators. *Phys. Rev. Lett.* **112**, 056804 (2014).
92. Wilson, J. H., Allocca, A. A. & Galitski, V. Repulsive Casimir force between Weyl semimetals. *Phys. Rev. B* **91**, 235115 (2015).
93. Rodriguez-Lopez, P., Popescu, A., Fialkovsky, I., Khusnutdinov, N. & Woods, L. M. Signatures of complex optical response in Casimir interactions of type I and II Weyl semimetals. *Commun. Mater.* **1**, 14 (2020).
94. Woods, L. M. et al. Materials perspective on Casimir and van der Waals interactions. *Rev. Mod. Phys.* **88**, 045003 (2016).
95. fialkovsky, I., Khusnutdinov, N. & Vassilevich, D. Quest for Casimir repulsion between Chern–Simons surfaces. *Phys. Rev. B* **97**, 165432 (2018).
96. Vassilevich, D. On the (im)possibility of Casimir repulsion between Chern–Simons surfaces. *Mod. Phys. Lett. A* **35**, 2040017 (2020).
97. Martín-Ruiz, A., Cambiaso, M. & Urrutia, L. F. A Green's function approach to the Casimir effect on topological insulators with planar symmetry. *Europhys. Lett.* **113**, 60005 (2016).
98. Fukushima, K., Imaki, S. & Qiu, Z. Anomalous Casimir effect in axion electrodynamics. *Phys. Rev. D* **100**, 045013 (2019).
99. Hehl, F. W., Obukhov, Y. N., Rivera, J.-P. & Schmid, H. Magnetoelectric Cr_2O_3 and relativity theory. *Eur. Phys. J. B* **71**, 321–329 (2009).
100. Kurumaji, T. et al. Optical magnetoelectric resonance in a polar magnet $(Fe,Zn)_2Mo_3O_8$ with axion-type coupling. *Phys. Rev. Lett.* **119**, 077206 (2017).
101. Varnava, N., Souza, I. & Vanderbilt, D. Axion coupling in the hybrid Wannier representation. *Phys. Rev. B* **101**, 155130 (2020).
102. Maciejko, J., Qi, X.-L., Karch, A. & Zhang, S.-C. Fractional topological insulators in three dimensions. *Phys. Rev. Lett.* **105**, 246809 (2010).
103. Shi, W. et al. A charge-density-wave Weyl semimetal. Preprint at *arXiv* https://arxiv.org/abs/1909.04037 (2019).
104. Otrokov, M. M. et al. Prediction and observation of an antiferromagnetic topological insulator. *Nature* **576**, 416–422 (2019).
Combined theoretical and experimental study on antiferromagnetic topological insulator $MnBi_2Te_4$.
105. Gong, Y. et al. Experimental realization of an intrinsic magnetic topological insulator. *Chin. Phys. Lett.* **36**, 076801 (2018).
106. Hu, C. et al. A van der Waals antiferromagnetic topological insulator with weak interlayer magnetic coupling. *Nat. Commun.* **11**, 97 (2020).
107. Lv, B., Qian, T. & Ding, H. Angle-resolved photoemission spectroscopy and its application to topological materials. *Nat. Rev. Phys.* **1**, 609–626 (2019).
108. Lee, S. H. et al. Spin scattering and noncollinear spin structure-induced intrinsic anomalous Hall effect in antiferromagnetic topological insulator $MnBi_2Te_4$. *Phys. Rev. Res.* **1**, 012011 (2019).
109. Yan, J.-Q. et al. Crystal growth and magnetic structure of $MnBi_2Te_4$. *Phys. Rev. Mater.* **3**, 064202 (2019).
110. Chen, B. et al. Intrinsic magnetic topological insulator phases in the Sb doped $MnBi_2Te_4$ bulks and thin flakes. *Nat. Commun.* **10**, 4469 (2019).
111. Deng, Y. et al. Quantum anomalous Hall effect in intrinsic magnetic topological insulator $MnBi_2Te_4$. *Science* **367**, 895–900 (2020).
112. Otrokov, M. et al. Unique thickness-dependent properties of the van der Waals interlayer antiferromagnet $MnBi_2Te_4$ films. *Phys. Rev. Lett.* **122**, 107202 (2019).
113. Li, H. et al. Antiferromagnetic topological insulator $MnBi_2Te_4$: synthesis and magnetic properties. *Phys. Chem. Chem. Phys.* **22**, 556–563 (2020).
114. Li, Y. et al. Layer-magnetization-tuned topological phases in $Mn_2Bi_2Te_5$ films. Preprint at *arXiv* https://arxiv.org/abs/2001.06133 (2020).
115. Hao, Y.-J. et al. Gapless surface Dirac cone in antiferromagnetic topological insulator $MnBi_2Te_4$. *Phys. Rev. X* **9**, 041038 (2019).
116. Li, H. et al. Dirac surface states in intrinsic magnetic topological insulators $EuSn_2As_2$ and $MnBi_{2n}Te_{3n+1}$. *Phys. Rev. X* **9**, 041039 (2019).
117. Lee, D. S. et al. Crystal structure, properties and nanostructuring of a new layered chalcogenide semiconductor, Bi_2MnTe_4. *CrystEngComm* **15**, 5532–5538 (2013).
118. Swatek, P. et al. Gapless Dirac surface states in the antiferromagnetic topological insulator $MnBi_2Te_4$. *Phys. Rev. B* **101**, 161109 (2020).
119. Li, H. et al. Dirac surface states in intrinsic magnetic topological insulators $EuSn_2As_2$ and $MnBi_{2n}Te_{3n+1}$. *Phys. Rev. X* **9**, 041039 (2019).
120. Li, J. et al. Intrinsic magnetic topological insulators in van der Waals layered $MnBi_2Te_4$-family materials. *Sci. Adv.* **5**, eaaw5685 (2019).
121. Fei, R., Song, W. & Yang, L. Giant photogalvanic effect and second-harmonic generation in magnetic axion insulators. *Phys. Rev. B* **102**, 035440 (2020).
122. Wu, J. et al. Natural van der Waals heterostructural single crystals with both magnetic and topological properties. *Sci. Adv.* **5**, eaax9989 (2019).
123. Li, Y. et al. Layer-magnetization-tuned topological phases in $Mn_2Bi_2Te_5$ films. Preprint at *arXiv* https://arxiv.org/abs/2001.06133 (2020).
124. Hou, Y. S., Kim, J. W. & Wu, R. Q. Axion insulator state in ferromagnetically ordered $Cri_3/Bi_2Se_3/MnBi_2Se_4$ heterostructures. *Phys. Rev. B* **101**, 121401 (2020).
125. Li, Z. et al. Tunable interlayer magnetism and band topology in van der Waals heterostructures of $MnBi_2Te_4$-family materials. *Phys. Rev. B* **102**, 081107 (2020).
126. Wang, H. et al. Dynamical axion state with hidden pseudospin Chern numbers in $MnBi_2Te_4$-based heterostructures. *Phys. Rev. B* **101**, 081109 (2020).
127. Fu, H., Liu, C.-X. & Yan, B. Exchange bias and quantum anomalous Hall effect in the $MnBi_2Te_4/CrI_3$ heterostructure. *Sci. Adv.* **6**, eaaz0948 (2020).
128. Xu, Y., Song, Z., Wang, Z., Weng, H. & Dai, X. Higher-order topology of the axion insulator $EuIn_2As_2$. *Phys. Rev. Lett.* **122**, 256402 (2019).
129. Zhang, Y. et al. In-plane antiferromagnetic moments and magnetic polaron in the axion topological insulator candidate $EuIn_2As_2$. *Phys. Rev. B* **101**, 205126 (2020).
130. Regmi, S. et al. Temperature dependent electronic structure in a higher order topological insulator candidate $EuIn_2As_2$. Preprint at *arXiv* https://arxiv.org/abs/1911.03703 (2019).
131. Gui, X. et al. A new magnetic topological quantum material candidate by design. *ACS Central Sci.* **5**, 900–910 (2019).
132. Hou, Y. & Wu, R. Axion insulator state in a ferromagnet/topological insulator/antiferromagnet heterostructure. *Nano Lett.* **19**, 2472–2477 (2019).
133. Wieder, B. J., Lin, K.-S. & Bradlyn, B. Is the dynamical axion Weyl-charge-density wave an axionic band insulator? Preprint at *arXiv* https://arxiv.org/abs/2004.11401 (2020).
134. Wan, X., Turner, A., Vishwanath, A. & Savrasov, S. Y. Electronic structure of pyrochlore iridates: from topological Dirac metal to Mott insulator. *Phys. Rev. B* **83**, 205101 (2011).
135. Chen, G. & Hermele, M. Magnetic orders and topological phases from *f–d* exchange in pyrochlore iridates. *Phys. Rev. B* **86**, 235129 (2012).
136. Yamaura, J. et al. Tetrahedral magnetic order and the metal–insulator transition in the pyrochlore lattice of $Cd_2Os_2O_7$. *Phys. Rev. Lett.* **108**, 247205 (2012).
137. Shi, Y. G. et al. Continuous metal–insulator transition of the antiferromagnetic perovskite $NaOsO_3$. *Phys. Rev. B* **80**, 161104 (2009).
138. Liu, C. et al. Metallic surface electronic state in half-Heusler compounds RPtBi (R=Lu, Dy, Gd). *Phys. Rev. B* **83**, 205133 (2011).
139. Kreyssig, A. et al. Magnetic order in GdBiPt studied by X-ray resonant magnetic scattering. *Phys. Rev. B* **84**, 220408 (2011).
140. Müller, R. A. et al. Magnetic structure of GdBiPt: a candidate antiferromagnetic topological insulator. *Phys. Rev. B* **90**, 041109 (2014).
141. Gooth, J. et al. Experimental signatures of the mixed axial-gravitational anomaly in the Weyl semimetal NbP. *Nature* **547**, 324–327 (2017).
142. Ikebe, Y. et al. Optical hall effect in the integer quantum Hall regime. *Phys. Rev. Lett.* **104**, 256802 (2010).
143. Shimano, R. et al. Quantum Faraday and Kerr rotations in graphene. *Nat. Commun.* **4**, 1–6 (2013).
144. Mogi, M. et al. Tailoring tricolor structure of magnetic topological insulator for robust axion insulator. *Sci. Adv.* **3**, eaao1669 (2017).
145. Grauer, S. et al. Scaling of the quantum anomalous Hall effect as an indicator of axion electrodynamics. *Phys. Rev. Lett.* **118**, 246801 (2017).
146. Lachman, E. O. et al. Observation of superparamagnetism in coexistence with quantum anomalous Hall $C=\pm1$ and $C=0$ Chern states. *npj Quantum Mater.* **2**, 1–7 (2017).
147. Liu, C. et al. Robust axion insulator and Chern insulator phases in a two-dimensional antiferromagnetic topological insulator.*Nat. Mater.* **19**, 522–527 (2020).
148. Zhang, Y., Lin, L.-F., Moreo, A., Dong, S. & Dagotto, E. First-principles study of the low-temperature charge density wave phase in the quasi-one-dimensional Weyl chiral compound $(TaSe_4)_2I$. *Phys. Rev. B* **101**, 174106 (2020).
149. Marsh, D. J. E., Fong, K. C., Lentz, E. W., Šmejkal, L. & Ali, M. N. Proposal to detect dark matter using axionic topological antiferromagnets. *Phys. Rev. Lett.* **123**, 121601 (2019).
Proposal for a dark-matter axion detector based on an antiferromagnetic topological insulator.
150. Ringwald, A. Exploring the role of axions and other wisps in the dark Universe. *Phys. Dark Universe* **1**, 116–135 (2012).
151. Hofmann, J. & Sarma, S. D. Surface plasmon polaritons in topological Weyl semimetals. *Phys. Rev. B* **93**, 241402 (2016).
152. Zhao, B., Guo, C., Garcia, C. A. C., Narang, P. & Fan, S. Axion-field-enabled nonreciprocal thermal radiation in Weyl semimetals. *Nano Lett.* **20**, 1923–1927 (2020).
Exploitation of the axion field in an ideal Weyl semimetal for non-reciprocal thermal emitters.
153. Green, M. A. Time-asymmetric photovoltaics. *Nano Lett.* **12**, 5985–5988 (2012).
154. Soh, J.-R. et al. Ideal Weyl semimetal induced by magnetic exchange. *Phys. Rev. B* **100**, 201102 (2019).
155. Qi, X.-L., Witten, E. & Zhang, S.-C. Axion topological field theory of topological superconductors. *Phys. Rev. B* **87**, 134519 (2013).
156. Chen, C.-Z., Xie, Y.-M., Liu, J., Lee, P. A. & Law, K. T. Quasi-one-dimensional quantum anomalous Hall systems as new platforms for scalable topological quantum computation. *Phys. Rev. B* **97**, 104504 (2018).
157. Lian, B., Sun, X.-Q., Vaezi, A., Qi, X.-L. & Zhang, S.-C. Topological quantum computation based on chiral Majorana fermions. *Proc. Natl Acad. Sci. USA* **115**, 10938–10942 (2018).
158. Burkov, A. A. Topological semimetals. *Nat. Mater.* **15**, 1145–1148 (2016).
159. Keimer, B. & Moore, J. E. The physics of quantum materials. *Nat. Phys.* **13**, 1045–1055 (2017).
160. Altland, A. & Zirnbauer, M. R. Nonstandard symmetry classes in mesoscopic normal–superconducting hybrid structures. *Phys. Rev. B* **55**, 1142–1161 (1997).
161. Kitaev, A. Periodic table for topological insulators and superconductors. *AIP Conf. Proc.* **1134**, 22–30 (2009).
162. Chern, S.-S. & Simons, J. Characteristic forms and geometric invariants. *Ann. Math.* **99**, 48–69 (1974).
163. Witten, E. Topological quantum field theory. *Commun. Math. Phys.* **117**, 353–386 (1988).
164. Hsiang, W.-Y. & Lee, D.-H. Chern–Simons invariant in the Berry phase of a 2x2 Hamiltonian. *Phys. Rev. A* **64**, 052101 (2001).
165. Chiu, C.-K., Teo, J. C. Y., Schnyder, A. P. & Ryu, S. Classification of topological quantum matter with symmetries. *Rev. Mod. Phys.* **88**, 035005 (2016).
166. Adler, S. L. Axial-vector vertex in spinor electrodynamics. *Phys. Rev.* **177**, 2426–2438 (1969).
167. Bell, J. S. & Jackiw, R. A PCAC puzzle. *Nuovo Cim. A* **60**, 47–61 (1969).
168. Chen, Y., Wu, S. & Burkov, A. A. Axion response in Weyl semimetals. *Phys. Rev. B* **88**, 125105 (2013).
169. Goswami, P. & Tewari, S. Axionic field theory of (3+1)-dimensional Weyl semimetals. *Phys. Rev. B* **88**, 245107 (2013).
170. Liang, S. et al. Experimental tests of the chiral anomaly magnetoresistance in the Dirac–Weyl semimetals Na_3Bi and GdPtBi. *Phys. Rev. X* **8**, 031002 (2018).

Acknowledgements
The authors thank Y. Wang (Harvard) and S. Roychowdhury (Max Planck Institute) for input and discussions. This work was supported by the US Department of Energy 'Photonics at Thermodynamic Limits' Energy Frontier Research Center under grant DE-SC0019140, the Army Research Office MURI (Ab-Initio Solid-State Quantum Materials) grant no. W911NF-18-1-0431 and by the Science and Technology Center (STC) Center for Integrated Quantum Materials under US National Science Foundation (NSF) grant no. DMR-1231319. C.A.C.G. is supported by the NSF Graduate Research Fellowship Program under grant no. DGE-1745303. Financial support by the European Union (grant no. 742068) is gratefully acknowledged. P.N. is a Moore Inventor Fellow and gratefully acknowledges support through grant no. GBMF8048 from the Gordon and Betty Moore Foundation.

Author contributions
The authors contributed equally to all aspects of the article.

Competing interests
The authors declare no competing interests.

Peer review information
Nature Reviews Physics thanks Pavan Hosur and the other, anonymous, reviewer(s) for their contribution to the peer review of this work.

Publisher's note
Springer Nature remains neutral with regard to jurisdictional claims in published maps and institutional affiliations.